

Magnetomotive nanoparticle transducers for optical rheology of viscoelastic materials

Vasilica Crecea,^{1,2} Amy L. Oldenburg,^{2,3,4} Xing Liang,^{2,3} Tyler S. Ralston,^{2,3,5} and Stephen A. Boppart^{2,3,6,*}

¹Department of Physics, University of Illinois at Urbana-Champaign, 1110 W. Green St., Urbana, IL 61801, USA

²Beckman Institute for Advanced Science and Technology, University of Illinois at Urbana-Champaign, 405 N. Mathews Ave., Urbana, IL 61801, USA

³Department of Electrical and Computer Engineering, University of Illinois at Urbana-Champaign, 1406 W. Green St., Urbana, IL 61801, USA

⁴Current address: Department of Physics and Astronomy, University of North Carolina, Chapel Hill, NC 27599-3255, USA

⁵Current address: Lincoln Laboratory, Massachusetts Institute of Technology, 244 Wood St., Lexington, MA 02420-9108, USA

⁶Department of Bioengineering, University of Illinois at Urbana-Champaign, 1304 West Springfield Avenue, Urbana, IL 61801, USA

*boppart@illinois.edu

Abstract: The availability of a real-time non-destructive modality to interrogate the mechanical properties of viscoelastic materials would facilitate many new investigations. We introduce a new optical method for measuring elastic properties of samples which employs magnetite nanoparticles as perturbative agents. Magnetic nanoparticles distributed in silicone-based samples are displaced upon probing with a small external magnetic field gradient and depth-resolved optical coherence phase shifts allow for the tracking of scatterers in the sample with nanometer-scale sensitivity. The scatterers undergo underdamped oscillations when the magnetic field is applied step-wise, allowing for the measurement of the natural frequencies of oscillation of the samples. Validation of the measurements is accomplished using a commercial indentation apparatus to determine the elastic moduli of the samples. This real-time non-destructive technique constitutes a novel way of probing the natural frequencies of viscoelastic materials in which magnetic nanoparticles can be introduced.

©2009 Optical Society of America

OCIS codes: (170.4500) Optical coherence tomography; (120.5820) Scattering measurements; (120.5050) Phase measurement; (160.3820) Magneto-optical materials.

References

1. N. W. Tschoegl, *The phenomenological theory of linear viscoelastic behavior: an introduction* (Springer-Verlag, 1989).
2. A. Wineman, and K. Rajagopal, *Mechanical Response of Polymers* (Cambridge University Press, 2000).
3. J. Ferry, *Viscoelastic Properties of Polymers* (John Wiley and Sons, 1980).
4. D. Ouis, "Characterization of polymers by means of a standard viscoelastic model and fractional derivative calculus," *Int. J. Polym. Mater.* **53**(8), 633–644 (2004).
5. M. Sridhar, J. Liu, and M. F. Insana, "Elasticity imaging of polymeric media," *J. Biomech. Eng.* **129**(2), 259–272 (2007).
6. J. F. Greenleaf, M. Fatemi, and M. Insana, "Selected methods for imaging elastic properties of biological tissues," *Annu. Rev. Biomed. Eng.* **5**(1), 57–78 (2003).
7. J. Ophir, S. K. Alam, B. S. Garra, F. Kallel, E. E. Konofagou, T. Krouskop, C. R. B. Merritt, R. Righetti, R. Souchon, S. Srinivasan, and T. Varghese, "Elastography: imaging the elastic properties of soft tissues with ultrasound," *J. Med. Ultrasound* **29**(4), 155–171 (2002).
8. I. Céspedes, J. Ophir, H. Ponnekanti, and N. Maklad, "Elastography: elasticity imaging using ultrasound with application to muscle and breast *in vivo*," *Ultrason. Imaging* **15**(2), 73–88 (1993).
9. R. Muthupillai, D. J. Lomas, P. J. Rossman, J. F. Greenleaf, A. Manduca, and R. L. Ehman, "Magnetic resonance elastography by direct visualization of propagating acoustic strain waves," *Science* **269**(5232), 1854–1857 (1995).

10. A. Manduca, T. E. Oliphant, M. A. Dresner, J. L. Mahowald, S. A. Kruse, E. Amromin, J. P. Felmlee, J. F. Greenleaf, and R. L. Ehman, "Magnetic resonance elastography: *in vivo* non-invasive mapping of tissue elasticity," *Med. Image Anal.* **5**(4), 237–254 (2001).
11. A. J. Romano, J. A. Bucaro, R. L. Ehman, and J. J. Shirron, "Evaluation of a material parameter extraction algorithm using MRI-based displacement measurements," *IEEE Trans. Ultrason. Ferroelectr. Freq. Control* **47**(6), 1575–1581 (2000).
12. R. Sinkus, M. Tanter, S. Catheline, J. Lorenzen, C. Kuhl, E. Sondermann, and M. Fink, "Imaging anisotropic and viscous properties of breast tissue by magnetic resonance-elastography," *Magn. Reson. Med.* **53**(2), 372–387 (2005).
13. O. V. Rudenko, A. P. Sarvazyan, and S. Y. Emelianov, "Acoustic radiation force and streaming induced by focused nonlinear ultrasound in a dissipative medium," *J. Acoust. Soc. Am.* **99**(5), 2791–2798 (1996).
14. S. Chen, M. Fatemi, and J. F. Greenleaf, "Remote measurement of material properties from radiation force induced vibration of an embedded sphere," *J. Acoust. Soc. Am.* **112**(3 Pt 1), 884–889 (2002).
15. C. Reynaud, F. Sommer, C. Quet, N. El Bounia, and T. M. Duc, "Quantitative determination of Young's modulus on a biphasic polymer system using atomic force microscopy," *Surf. Interface Anal.* **30**(1), 185–189 (2000).
16. J. M. Schmitt, "OCT elastography: imaging microscopic deformation and strain of tissue," *Opt. Express* **3**(6), 199–211 (1998).
17. A. S. Khalil, R. C. Chan, A. H. Chau, B. E. Bouma, and M. R. Mofrad, "Tissue elasticity estimation with optical coherence elastography: toward mechanical characterization of *in vivo* soft tissue," *Ann. Biomed. Eng.* **33**(11), 1631–1639 (2005).
18. G. van Soest, F. Mastik, N. de Jong, and A. F. W. van der Steen, "Robust intravascular optical coherence elastography by line correlations," *Phys. Med. Biol.* **52**(9), 2445–2458 (2007).
19. J. Rogowska, N. A. Patel, J. G. Fujimoto, and M. E. Brezinski, "Optical coherence tomographic elastography technique for measuring deformation and strain of atherosclerotic tissues," *Heart* **90**(5), 556–562 (2004).
20. H. J. Ko, W. Tan, R. Stack, and S. A. Boppart, "Optical coherence elastography of engineered and developing tissue," *Tissue Eng.* **12**(1), 63–73 (2006).
21. R. K. Wang, S. J. Kirkpatrick, and M. Hinds, "Phase-sensitive optical coherence elastography for mapping tissue microstrains in real time," *Appl. Phys. Lett.* **90**(16), 164105 (2007).
22. S. J. Kirkpatrick, R. K. Wang, and D. D. Duncan, "OCT-based elastography for large and small deformations," *Opt. Express* **14**(24), 11585–11597 (2006).
23. A. L. Oldenburg, J. R. Gunther, and S. A. Boppart, "Imaging magnetically labeled cells with magnetomotive optical coherence tomography," *Opt. Lett.* **30**(7), 747–749 (2005).
24. E. P. Furlani, "Magnetophoretic separation of blood cells at the microscale," *J. Phys. D Appl. Phys.* **40**(5), 1313–1319 (2007).
25. R. Leitgeb, C. K. Hitzenberger, and A. F. Fercher, "Performance of fourier domain vs. time domain optical coherence tomography," *Opt. Express* **11**(8), 889–894 (2003).
26. A. L. Oldenburg, F. J. J. Touban, K. S. Suslick, A. Wei, and S. A. Boppart, "Magnetomotive contrast for *in vivo* optical coherence tomography," *Opt. Express* **13**(17), 6597–6614 (2005).
27. V. Crecea, A. L. Oldenburg, T. S. Ralston, and S. A. Boppart, "Phase-resolved spectral-domain magnetomotive optical coherence tomography," *Proc. SPIE* **6429**, 64291X (2007).
28. A. L. Oldenburg, V. Crecea, S. A. Rinne, and S. A. Boppart, "Phase-resolved magnetomotive OCT for imaging nanomolar concentrations of magnetic nanoparticles in tissues," *Opt. Express* **16**(15), 11525–11539 (2008).
29. D. C. Adler, R. Huber, and J. G. Fujimoto, "Phase-sensitive optical coherence tomography at up to 370,000 lines per second using buffered Fourier domain mode-locked lasers," *Opt. Lett.* **32**(6), 626–628 (2007).
30. A. M. Zysk, E. J. Chaney, and S. A. Boppart, "Refractive index of carcinogen-induced rat mammary tumours," *Phys. Med. Biol.* **51**(9), 2165–2177 (2006).
31. D. Valtorta, and E. Mazza, "Dynamic measurement of soft tissue viscoelastic properties with a torsional resonator device," *Med. Image Anal.* **9**(5), 481–490 (2005).
32. X. Liang, A. L. Oldenburg, V. Crecea, E. J. Chaney, and S. A. Boppart, "Optical micro-scale mapping of dynamic biomechanical tissue properties," *Opt. Express* **16**(15), 11052–11065 (2008).
33. A. Samani, J. Bishop, C. Luginbuhl, and D. B. Plewes, "Measuring the elastic modulus of *ex vivo* small tissue samples," *Phys. Med. Biol.* **48**(14), 2183–2198 (2003).
34. P. Agache, and P. Humbert, *Measuring the skin* (Springer-Verlag, 2004).

1. Introduction

Viscoelastic materials are omnipresent, including shock attenuation devices in car mechanics, soil which influences the settlement of buildings, vibration controllers in computer hard drives, sound absorbers, and cells and tissues within biological systems. Viscoelastic materials, as their name suggests, have both elastic and viscous properties. Namely, they store a portion of the energy they receive from external sources as potential energy, while the other portion is damped [1–5]. Their mechanical properties are of crucial importance for their function and reliability, a fact well known in the materials science field where high-performance materials are widely sought. One field of study that aims to characterize the mechanical properties of materials is rheology, widely known to address the change in form

and the flow of matter. In the bioimaging field, elastography is a technique for the measurement of elasticity of biomaterials, which are most often viscoelastic.

Current methods for the measurement of mechanical properties of viscoelastic materials include ultrasound elastography [5–8], magnetic resonance elastography [9–12], vibroacoustography [13,14], atomic force microscopy (AFM) [15], and optical coherence elastography [16–22]. These methods are either static or dynamic, and aim to detect displacements in samples when an external or internal stress is applied. Computational cross-correlation algorithms are often employed for tracking image features or pixels, and mapping their displacement [10,16]. Unfortunately, these algorithms are prone to error in accurately measuring displacements and tracking of scatterers [10]. The inability to obtain quantitative measurements and the need for reference samples that yield relative measurements are some of the more common disadvantages of some of these techniques. Elastography imaging systems typically require high cost and long data acquisition and processing times [6–15]. A more traditional technique for measuring mechanical properties of samples is indentation, wherein controlled mechanical pressure is applied to samples with well-defined geometries and the strain-stress curves are used for inferring the bulk elastic moduli of the probed samples. Elastography and rheology, both well-established fields, have been greatly advanced by new technologies for characterizing material properties, and in particular, viscoelastic parameters. These advances have been limited, however, by challenges such as resolution or the need to isolate the samples for measurements. The need for an inexpensive, real-time, non-contact, non-destructive, and quantitative method for the assessment of highly localized micromechanical properties with few constraints on the geometry or dimensions of the samples is apparent.

We propose a fundamentally new approach for probing the micromechanical properties and microenvironments of viscoelastic materials. By introducing magnetic nanoparticles (MNPs) in the medium to be probed, and by applying a small, controlled, external magnetic field, one gains access to the nano- to micro-level interactions between the MNPs and the surrounding microenvironmental matrix [23,24].

In this paper we introduce a novel optical elastography technique, magnetomotive optical coherence elastography (MM-OCE), based on phase-resolved spectral-domain optical coherence tomography (OCT) [25] which affords the capability of imaging non-invasively, non-destructively, and in real time. Micromechanical properties of samples can be determined from dynamic measurements when a controlled modulated mechanical response is triggered in the sample [23,26–28]. Magnetomotion is induced in silicone-based samples via the interaction of a small localized external magnetic field with MNPs distributed in the samples. This novel technique combines the advantages of localized magnetomotive contrast on the micron scale with fast real-time depth-resolved optical imaging to quantify the dynamic micromechanical properties of viscoelastic materials. Magnetomotive optical coherence elastography is conceptually different from magnetomotive OCT (MM-OCT) [23,26,28] because it quantitatively measures the time-dependent oscillations of MNPs and their surrounding microenvironment, and uses this information to determine the viscoelastic properties of the medium. In contrast, MM-OCT only uses the MNP modulation as a means for contrast enhancement in OCT.

2. Methods and results

In order to assess the validity of MM-OCE for measuring dynamic elastic properties of materials with different stiffness, we examined a set of polymer-based samples with elastic mechanical properties that spanned a wide range. Polydimethylsiloxane (PDMS)-based samples with optical and mechanical properties representative of soft polymers, composites, and biological tissues were prepared [4]. To vary the elasticity of the samples, the ratio (PDMS):(curing agent RTV 615 A) was varied in the range 25:1-10:1, while the relative ratio of the curing agent and the crosslinker, RTV 615 A:RTV 615 B, was maintained at 10:1 for all samples. Titanium dioxide (TiO_2) microparticles (Sigma-Aldrich, #224227, average diameter 1 μm , < 5 μm) with a concentration of 4 mg/g served as optical scatterers and

magnetite MNPs (average diameter 25 nm, Sigma-Aldrich, #637106) with a concentration of 2 mg/g served as magnetomotive perturbative agents. The polymers and the TiO₂ particles were thoroughly mixed with the aid of a magnetic stir plate. Subsequently, the MNPs were added and the sample solution was homogenized in an ultrasonic sonicator for five hours. They were then poured into Petri dishes with a diameter of 38 mm and a height of 5 mm, curing 12 hrs at 80°C, and subsequently 24 hr at room temperature (22 °C). An indentation instrument (model TA.XT Plus Texture Analyzer, Texture Technologies Corp., Algonquin, IL) was used for independent validation measurements of the elastic moduli of the samples.

The composition of these samples was varied, resulting in noticeable (by palpation) differences in their elasticity. As confirmed by indentation measurements using a commercial indentation instrument, the static elastic moduli of these samples ranged from 0.4 to 140 kPa. The concentration of optical scatterers and MNPs as well as the geometry and dimensions of all samples were kept constant. In this study, the MNPs are believed to be mechanically bound directly to the solid polymer matrix of the silicone medium. The consistency and repeatability of the MM-OCE measurements support this hypothesis.

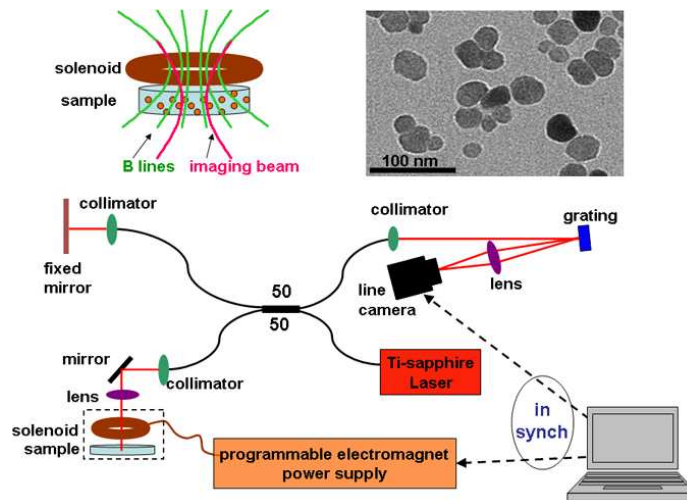


Fig. 1. Schematic diagram of the MM-OCE set up with MNPs. (top left) The magnetic coil provides a magnetic field that is aligned axially with the imaging beam. The field gradient engages the motion of MNPs in the sample. (top right) Transmission electron micrograph of the magnetite MNPs. (bottom) The near-infrared light provided by the titanium:sapphire laser is divided by the 50:50 fiber-optic beamsplitter between the reference and the sample arms of the interferometer. The interference signal is wavelength-dispersed by a diffraction grating and recorded by a charged coupled device (CCD) line array. The magnetic field activity is synchronized with the OCT data acquisition, and the resulting optical back-scattering data is acquired, processed, and displayed on a personal computer.

A spectral-domain optical coherence tomography (OCT) system [23] was used to perform real-time interferometric imaging of the samples. The sample arm was modified to accommodate a small electromagnetic coil custom-designed to optimize the magnetic field gradient within the focal region of the optical imaging system, as illustrated in Fig. 1. The probing light was provided by a Nd:YVO₄-pumped titanium:sapphire laser (KMLabs, Boulder, CO) with a center wavelength of 800 nm and a bandwidth of 120 nm, providing an axial resolution of 3 μm in the samples. The average power incident on the samples was 10 mW. A 40 mm focal length lens was used to focus the light in the sample arm to a 16 μm spot (transverse resolution). Magnetic field modulation was synchronized with optical data acquisition. M-mode imaging data was acquired at a camera line rate of 29 kHz (34 μs per axial depth scan) for a total acquisition time of 280 ms per M-mode image. During the acquisition of each image the magnetic field was turned on shortly after the start of the

acquisition and kept constant for 100 ms, and then switched off in a square-wave pattern, releasing the MNPs and resulting in the relaxation of the sample, as illustrated in Fig. 2.

The complex analytic signal obtained from the raw optical data acquired in M-mode was used to extract the phase associated with individual scatterers in the samples (at fixed positions in depth) as a function of time. The phase variation was recorded as the magnetic field was applied step-wise to the sample, and the absolute displacement of the scatterers was deduced from Eq. (1) [29]:

$$d\varphi(dt) = \frac{4\pi n}{\lambda_0} dz(dt), \quad (1)$$

where dt is the time between consecutive axial scans, $d\varphi(dt)$ is the change in unwrapped phase (in radians [29]), n is the index of refraction of the silicone sample medium (1.44, as measured by OCT [30]), λ_0 is the center wavelength of the probing light (800 nm), and $dz(dt)$ is the displacement of each scatterer over dt . Based on the parameters of our system and of our samples, the displacement can be calculated directly from the equation above. The displacement sensitivity of the system, defined as the standard deviation of the measured position of a stationary mirror in the sample arm, was 11 nm. Typical maximum displacements measured in the samples were in the order of a few hundred nanometers.

Within 2-20 ms after the onset of the magnetic field, the scatterers were observed to reach a maximum displacement. This was followed by an underdamped oscillation (Fig. 2). If a steady magnetic field gradient was present, such as following a step-function change in the applied magnetic field gradient, the scatterers eventually settled to a new static position as they reached a new equilibrium position (data not shown). A similar behavior was observed when the field was removed and the MNPs in the sample were released from the magnetic force and allowed to oscillate around their initial equilibrium position as a result of the binding/restoring force on the MNP from the microenvironment. The settling of the particles to a new static position is not necessary for the measurements reported in this study. A few oscillation cycles are sufficient for determining the resonant frequency of the sample. The static positions in these samples were measured to be stable over hundreds of milliseconds.

The requirement for the linearity of the viscoelastic material behavior is that the displacements induced be at most 0.2% of the length of the sample [31]. In our case, the height of the samples was 5 mm, and therefore displacements of at most 10 μm would ensure a linear response and predict direct proportionality of natural frequencies with the square root of the elastic moduli. Moreover, in order to avoid confounding phase unwrapping, displacements did not exceed half the axial resolution of the OCT system, namely 1.5 μm . Therefore, the strength of the magnetic field was adjusted in the range of 100-600 Gauss for samples with different elasticities to ensure that this maximum displacement was not exceeded. The graph in Fig. 3 shows the variation of the maximum phase change and displacement in a representative sample (with an RTV A:RTV B ratio of 10:1, a concentration of 2.5 mg/g of MNPs, 4 mg/g TiO_2 and with a measured elastic modulus of 3.1 kPa) as the magnetic field strength is increased.

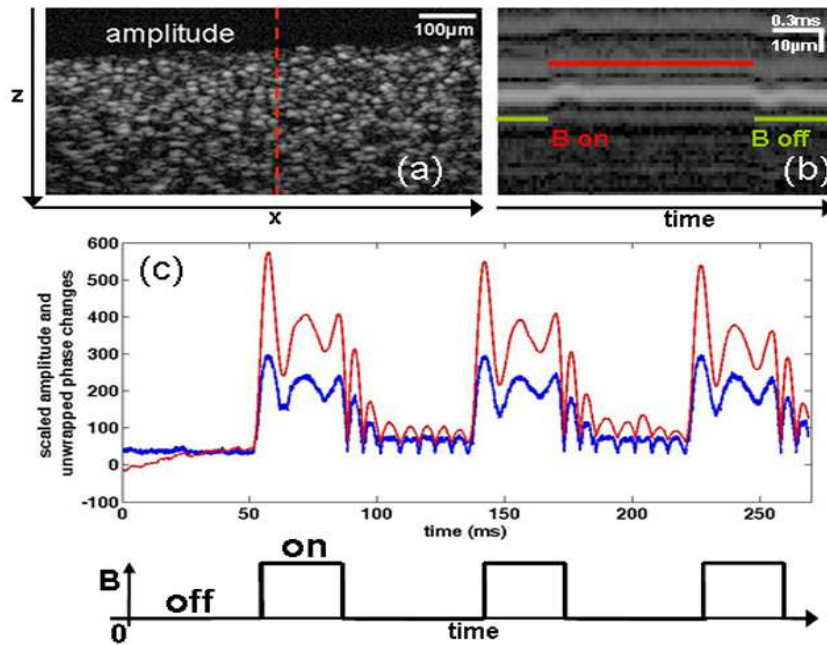


Fig. 2. Scatterer response upon square-wave modulation of a magnetic field. (a) Two-dimensional (x-z) cross-sectional (B-mode) amplitude OCT image of a silicone sample containing MNPs and TiO₂ optical scatterers. The dashed line indicates the location in the sample where M-mode imaging was performed with MM-OCE. (b) M-mode amplitude OCT image of a region of scatterers acquired while the magnetic field was applied in a square-wave pattern. (c) Average time-dependent scatterer changes along one axial position, illustrating both the changes in phase (red) and changes in amplitude (blue) as the magnetic field is applied, relative to an idle state with zero magnetic field.

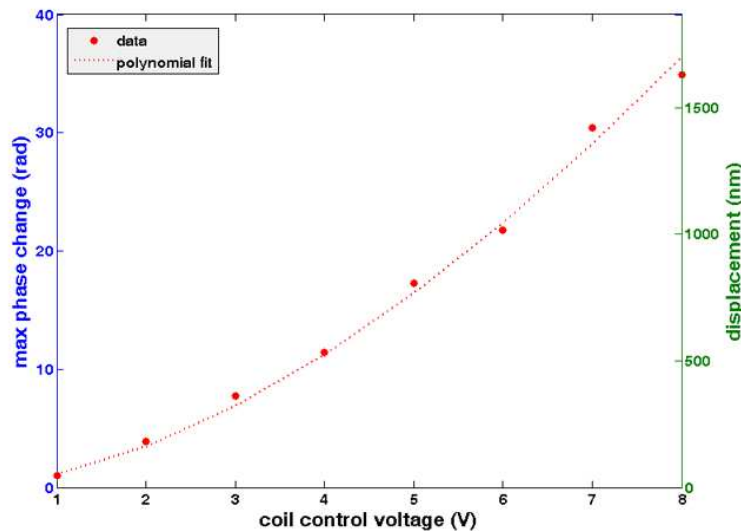


Fig. 3. Scatterer response to different magnetic field strengths. Direct measurements (points) of maximum change in unwrapped phase from an average scatterer, which are directly proportional to the average maximum displacements of the MNPs, as the electromagnet control voltage is changed. The polynomial fit follows the law $y = Cx^{1.7}$. The applied voltage is directly proportional to the gradient of the square of the magnetic field. MM-OCE data is acquired at displacements not exceeding 1.5 μm in order to avoid excessive phase wrapping of the phase signal.

The natural frequency of oscillation of each sample was obtained from the time-resolved displacement of each scatterer, measured optically with the coherence ranging system. The displacement curves of the scatterers were fitted to the equation of motion of an underdamped oscillator with two frequency components according to Eq. (2):

$$d(t) = \sum_{i=1}^2 a_i e^{-\gamma_i t} \cos(2\pi f_i t - \delta_i) + C, \quad (2)$$

where $d(t)$ is the displacement as a function of time, $a_{1,2}$ are the amplitudes of the two frequency components, $\gamma_{1,2}$ are the corresponding damping coefficients, $f_{1,2}$ are the frequencies of oscillation, $\delta_{1,2}$ are arbitrary phases, and C is a constant. The R-values of the curve fittings were all above 85%. The dominant natural frequencies of oscillation of the samples were plotted against the square root of the elastic modulus. Two frequency components were chosen in order to obtain a better fit of the displacement traces. These two frequency components are from an expected dominant longitudinal mode and possibly secondary harmonics or shear wave interference.

Figure 4 illustrates the normalized scatterer traces when the field was applied on three samples with different elastic moduli, as validated by indentation measurements. It is observed that the natural frequency of oscillation varies strongly with the elastic modulus and, as expected, stiffer samples exhibit higher frequencies. We note that some of the recorded displacement traces have secondary frequency components whose amplitudes are consistently smaller than those of the main frequency components.

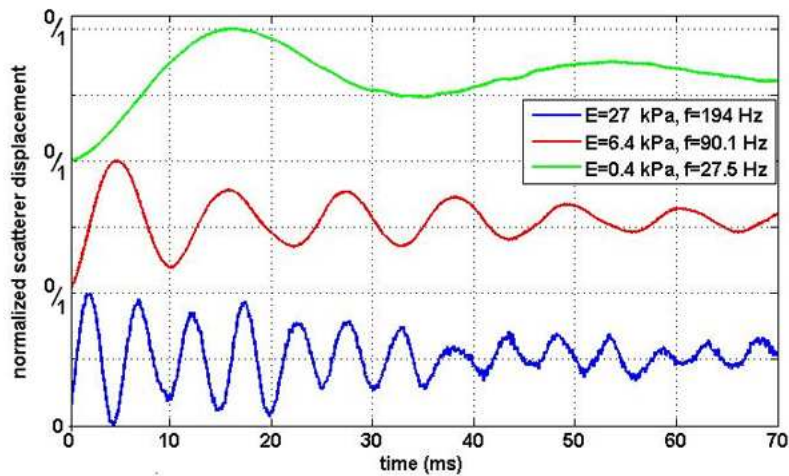


Fig. 4. Normalized measured displacements from samples of different elastic moduli following a step (off-to-on) transition of the applied magnetic field. Three samples that span a wide range of elastic moduli (measured by indentation: 0.4 kPa [green], 6.4 kPa [red], 27 kPa [blue]) are shown. These sample moduli are characteristic of soft biological tissue, and were chosen to illustrate the natural frequencies of oscillation measured by MM-OCE. The “0/1” labels on the vertical axis are respectively indicating the minimum and maximum of the normalized amplitudes of the displacements traces. As expected, it is observed that as the stiffness of the medium increases, the natural frequency of oscillation of the response increases.

3. Discussion

Viscoelastic media can often be modeled as a Voigt body [32]. This model predicts a linear relationship between the natural frequency of oscillation of a material and the square root of its elastic modulus. The graph in Fig. 5 summarizes the MM-OCE measurements of natural frequencies of oscillation for the range of samples investigated, with elastic moduli varying between 0.4 and 140 kPa, confirming this prediction. The natural frequencies closely follow a

linear dependence on the square root of the elastic moduli over this range that spans three orders of magnitude, reinforcing the validity and applicability of MM-OCE for elasticity measurements of various materials.

The range of elastic moduli investigated here was representative of the majority of soft polymer composites and matrices. It should be noted that studies have reported biological tissues also exhibit elastic moduli in a range similar to that investigated in this study, with representative values for adipose tissue (1.9 kPa), breast tumor (12 kPa) [33], and forearm skin (120 kPa) [34]. With the current MM-OCE technology, samples stiffer than 140 kPa exhibited an overdamped response when the magnetic field was applied, and the analysis presented in this paper does not apply in such cases. Samples softer than 0.4 kPa are similar to a liquefied gel and their frequencies of oscillation are too low to be measured in real-time with the MM-OCE system. However, the range of elasticities explored herein is representative for many materials of interest, demonstrating that MM-OCE has the potential for a wide range of investigational and diagnostic studies in materials science, biology, and medicine. MM-OCE requires that the magnetic nanoparticles be present in the samples. The magnetic nanoparticles used in this study, however, had a negligible effect on the bulk elastic modulus of the samples, as demonstrated by measurements with a commercial indentation instrument. Future modeling is needed to more precisely describe the dependence of the natural frequency of oscillation on the elastic modulus while taking into account the interactions between MNPs and their cooperative interactions with the external magnetic field, as well as how the binding of MNPs to the surrounding matrix affects the displacement of scatterers.

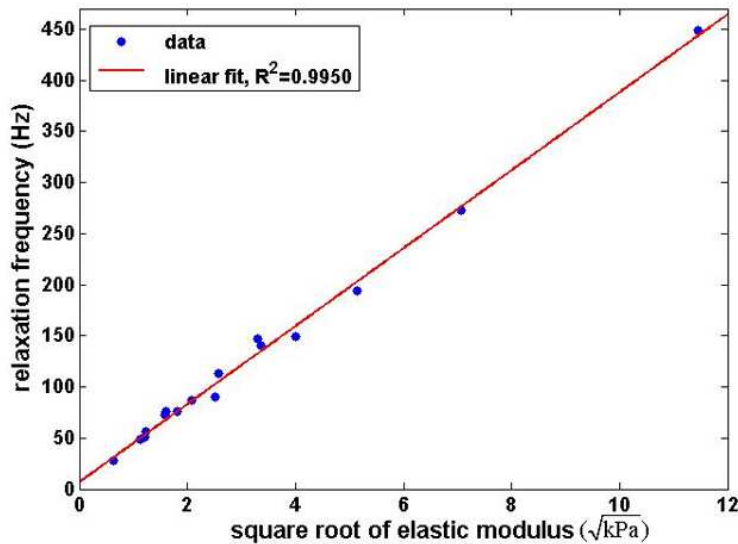


Fig. 5. MM-OCE-measured natural frequencies of oscillation in samples of varying elastic moduli. The natural frequency of oscillation of the viscoelastic medium depends linearly on the square root of the elastic modulus, as predicted by the Kelvin-Voigt model. The MM-OCE relaxation frequency data (vertical axis) were collected as the samples relaxed following an on-to-off step magnetic field transition. The elastic moduli (horizontal axis) values were measured by indentation.

MM-OCE benefits from nanometer displacement sensitivity due to phase stability in the optical ranging system and the fact that minute (sub-resolution) displacements of scatterers in the samples result in slight changes in phase. The error in the measurements of the frequencies of oscillation was as small as 0.03% and no larger than 2%. The main noise sources in the MM-OCE system are i) the small variations of the magnetic field gradient due to inhomogeneities in the field, the coil design, and the sample, ii) the scatterer movement in

the three-dimensional sample matrix due to sample material inhomogeneities, iii) the optical source and detection electronics with inherent intensity, thermal, and shot noise contributions, and iv) the fitting of the displacement traces which estimates the actual particle displacement. Given the high resolution and high sensitivity of the imaging system, MM-OCE can readily measure real-time displacements non-invasively and non-destructively at the micron level, without the requirement of physical contact with the sample. This offers a clear advantage over other mechanical methods that measure stress-strain characteristics and have these limitations.

Boundary conditions (such as the geometry and the dimensions of a sample) are generally important in assessing the values of elastic moduli. In our study, the boundary conditions were controlled and kept constant for all samples. It has been suggested, however, that dynamic methods for probing mechanical properties have the potential for local characterization regardless of boundary conditions (when the boundaries are relatively far from the point of measurement [6]). Efforts are currently being directed towards the development of analytical models that describe viscoelastic media and the dynamic regime that MM-OCE is probing, as well as towards the investigation of the effect of boundary conditions on the values of the natural frequencies of oscillation.

Phase-resolved methods employed for scatterer tracking in MM-OCE afford real-time nano- to micro-scale measurements, creating the possibility for mapping mechanical properties with high resolution, superior to that of most other rheology technologies. The utilization of MNPs in MM-OCE and their nanometer-scale displacements enables the interrogation of a medium of interest at the nano-level and, given the cooperative action of the MNPs, at the micro-level of the sample. MM-OCE can directly measure natural frequencies of oscillation of various samples. With this versatility, MM-OCE could become a powerful tool with a wide range of applications in materials science.

Acknowledgments

We thank Daniel L. Marks from the Beckman Institute for Advanced Science and Technology, University of Illinois at Urbana-Champaign, for his assistance with the optical system and for useful discussions. We also thank Michael F. Insana and Marko B. Orescanin for their assistance with the indentation measurements, and Narayana Aluru and his research team for helpful discussions. This work was supported in part by the National Institute of Health (Roadmap Initiative, NIBIB, R21 EB005321, and NIBIB, R01 EB009073, S.A.B.), and the National Science Foundation (BES 05-19920, S.A.B.). V.C. was partially supported by the Linda Su-Nan Chang Sah Doctoral Fellowship through the Department of Electrical and Computer Engineering, University of Illinois at Urbana-Champaign. Additional information can be found at <http://biophotonics.illinois.edu>.